Research Article | Vol. 25, No. 24 | 27 Nov 2017 | OPTICS EXPRESS A1154
Optics EXPRESS

All-inorganic perovskite-based distributed feedback resonator

JUNYI GONG,[1,5] YUE WANG,[2,5] SHENG LIU,[3] PAN ZENG,[1] XILU YANG,[1] RONGQING LIANG,[1,4] QIONGRONG OU,[1,4,6] XIANG WU,[3,7] AND SHUYU ZHANG[1,4,8]

[1]*Department of Light Sources and Illuminating Engineering, Fudan University, Shanghai 200433, China*
[2]*Department of Physics, University of York, York, YO10 5DD, UK*
[3]*Department of Optical Science and Engineering, and Shanghai Ultra-Precision Optical Manufacturing Engineering Center, Fudan University, Shanghai 200433, China*
[4]*Engineering Research Center of Advanced Lighting Technology, Ministry of Education, and Institute of Beyond Lighting, Academy for Engineering and Technology, Fudan University, Shanghai 200433, China*
[5]*contributed equally*
[6]*qrou@fudan.edu.cn*
[7]*wuxiang@fudan.edu.cn*
[8]*zhangshuyu@fudan.edu.cn*

Abstract: Halide perovskite materials have rapidly emerged as outstanding optoelectronic materials for solar cells, light-emitting diodes (LEDs), and lasers. Compared to hybrid organic-inorganic perovskites, all-inorganic perovskites have shown unique merits that may contribute to the ultimate goal of developing electrically-pumped lasers. In this paper, we demonstrate a distributed feedback (DFB) resonator using an all-inorganic perovskite thin film as the gain medium. The film has a gain coefficient of 161.1 cm^{-1} and a loss coefficient of 30.9 cm^{-1}. Excited by picosecond pulses, the microstructured all-inorganic perovskite film exhibits a single-mode emission at 654 nm with a threshold of 33 $\mu J/cm^2$. The facile fabrication process provides a promising route towards low-cost single-mode visible lasers for many practical applications.

OCIS codes: (140.3490) Lasers, distributed-feedback; (140.3380) Laser materials; (230.4000) Microstructure fabrication.

References and links

1. W. S. Yang, J. H. Noh, N. J. Jeon, Y. C. Kim, S. Ryu, J. Seo, and S. I. Seok, "High-performance photovoltaic perovskite layers fabricated through intramolecular exchange," Science **348**(6240), 1234–1237 (2015).
2. M. Saliba, T. Matsui, K. Domanski, J.-Y. Seo, A. Ummadisingu, S. M. Zakeeruddin, J.-P. Correa-Baena, W. R. Tress, A. Abate, A. Hagfeldt, and M. Grätzel, "Incorporation of rubidium cations into perovskite solar cells improves photovoltaic performance," Science **354**(6309), 206–209 (2016).
3. M. Saliba, T. Matsui, J.-Y. Seo, K. Domanski, J.-P. Correa-Baena, M. K. Nazeeruddin, S. M. Zakeeruddin, W. Tress, A. Abate, A. Hagfeldt, and M. Grätzel, "Cesium-containing triple cation perovskite solar cells: improved stability, reproducibility and high efficiency," Energy Environ. Sci. **9**(6), 1989–1997 (2016).
4. N. Wang, L. Cheng, R. Ge, S. Zhang, Y. Miao, W. Zou, C. Yi, Y. Sun, Y. Cao, R. Yang, Y. Wei, Q. Guo, Y. Ke, M. Yu, Y. Jin, Y. Liu, Q. Ding, D. Di, L. Yang, G. Xing, H. Tian, C. Jin, F. Gao, R. H. Friend, J. Wang, and W. Huang, "Perovskite light-emitting diodes based on solution-processed self-organized multiple quantum wells," Nat. Photonics **10**, 699–704 (2016).
5. L. Protesescu, S. Yakunin, M. I. Bodnarchuk, F. Krieg, R. Caputo, C. H. Hendon, R. X. Yang, A. Walsh, and M. V. Kovalenko, "Nanocrystals of Cesium Lead Halide Perovskites (CsPbX3, X = Cl, Br, and I): Novel Optoelectronic Materials Showing Bright Emission with Wide Color Gamut," Nano Lett. **15**(6), 3692–3696 (2015).
6. V. A. Hintermayr, A. F. Richter, F. Ehrat, M. Döblinger, W. Vanderlinden, J. A. Sichert, Y. Tong, L. Polavarapu, J. Feldmann, and A. S. Urban, "Tuning the Optical Properties of Perovskite Nanoplatelets through Composition and Thickness by Ligand-Assisted Exfoliation," Adv. Mater. **28**(43), 9478–9485 (2016).

#306076 https://doi.org/10.1364/OE.25.0A1154
Journal © 2017 Received 31 Aug 2017; revised 22 Oct 2017; accepted 31 Oct 2017; published 10 Nov 2017

Optics EXPRESS

7. G. Xing, B. Wu, X. Wu, M. Li, B. Du, Q. Wei, J. Guo, E. K. L. Yeow, T. C. Sum, and W. Huang, "Transcending the slow bimolecular recombination in lead-halide perovskites for electroluminescence," Nat. Commun. **8**, 14558 (2017).
8. G. Xing, N. Mathews, S. S. Lim, N. Yantara, X. Liu, D. Sabba, M. Grätzel, S. Mhaisalkar, and T. C. Sum, "Low-temperature solution-processed wavelength-tunable perovskites for lasing," Nat. Mater. **13**(5), 476–480 (2014).
9. F. Deschler, M. Price, S. Pathak, L. E. Klintberg, D.-D. Jarausch, R. Higler, S. Hüttner, T. Leijtens, S. D. Stranks, H. J. Snaith, M. Atatüre, R. T. Phillips, and R. H. Friend, "High Photoluminescence Efficiency and Optically Pumped Lasing in Solution-Processed Mixed Halide Perovskite Semiconductors," J. Phys. Chem. Lett. **5**(8), 1421–1426 (2014).
10. Q. Zhang, S. T. Ha, X. Liu, T. C. Sum, and Q. Xiong, "Room-Temperature Near-Infrared High-Q Perovskite Whispering-Gallery Planar Nanolasers," Nano Lett. **14**(10), 5995–6001 (2014).
11. B. R. Sutherland, S. Hoogland, M. M. Adachi, C. T. O. Wong, and E. H. Sargent, "Conformal Organohalide Perovskites Enable Lasing on Spherical Resonators," ACS Nano **8**(10), 10947–10952 (2014).
12. J. Xing, X. F. Liu, Q. Zhang, S. T. Ha, Y. W. Yuan, C. Shen, T. C. Sum, and Q. Xiong, "Vapor Phase Synthesis of Organometal Halide Perovskite Nanowires for Tunable Room-Temperature Nanolasers," Nano Lett. **15**(7), 4571–4577 (2015).
13. G. Xing, M. H. Kumar, W. K. Chong, X. Liu, Y. Cai, H. Ding, M. Asta, M. Grätzel, S. Mhaisalkar, N. Mathews, and T. C. Sum, "Solution-Processed Tin-Based Perovskite for Near-Infrared Lasing," Adv. Mater. **28**(37), 8191–8196 (2016).
14. M. D. McGehee, M. A. Díaz-García, F. Hide, R. Gupta, E. K. Miller, D. Moses, and A. J. Heeger, "Semiconducting polymer distributed feedback lasers," Appl. Phys. Lett. **72**, 1536–1538 (1998).
15. N. Tessler, G. J. Denton, and R. H. Friend, "Lasing from conjugated-polymer microcavities," Nature **382**, 695–697 (1996).
16. C. V. Shank, J. E. Bjorkholm, and H. Kogelnik, "Tunable distributed-feedback dye laser," Appl. Phys. Lett. **18**, 395–396 (1971).
17. M. Berggren, A. Dodabalapur, R. E. Slusher, A. Timko, and O. Nalamasu, "Organic solid-state lasers with imprinted gratings on plastic substrates," Appl. Phys. Lett. **72**, 410–411 (1998).
18. P. Brenner, M. Stulz, D. Kapp, T. Abzieher, U. W. Paetzold, A. Quintilla, I. A. Howard, H. Kalt, and U. Lemmer, "Highly stable solution processed metal-halide perovskite lasers on nanoimprinted distributed feedback structures", Appl. Phys. Lett. **109**, 141106 (2016).
19. M. Saliba, S. M. Wood, J. B. Patel, P. K. Nayak, J. Huang, J. A. Alexander-Webber, B. Wenger, S. D. Stranks, M. T. Hörantner, J. T.-W. Wang, R. J. Nicholas, L. M. Herz, M. B. Johnston, S. M. Morris, H. J. Snaith, and M. K. Riede, "Structured Organic-Inorganic Perovskite toward a Distributed Feedback Laser," Adv. Mater. **28**(5), 923–929 (2016).
20. G. L. Whitworth, J. R. Harwell, D. N. Miller, G. J. Hedley, W. Zhang, H. J. Snaith, G. A. Turnbull, and I. D. W. Samuel, "Nanoimprinted distributed feedback lasers of solution processed hybrid perovskites," Opt. Express **24**(21), 23677–23684 (2016).
21. H. Cha, S. Bae, H. Jung, M. J. Ko, and H. Jeon, "Single-Mode Distributed Feedback Laser Operation in Solution-Processed Halide Perovskite Alloy System," Adv. Opt. Mater. (posted 30 August 2017, in press).
22. J. R. Harwell, G. L. Whitworth, G. A. Turnbull, and I. D. W. Samuel, "Green Perovskite Distributed Feedback Lasers," Sci. Rep. **7**(1), 11727 (2017).
23. Y. Ling, Y. Tian, X. Wang, J. C. Wang, J. M. Knox, F. Perez-Orive, Y. Du, L. Tan, K. Hanson, B. Ma, and H. Gao, "Enhanced Optical and Electrical Properties of Polymer-Assisted All-Inorganic Perovskites for Light-Emitting Diodes," Adv. Mater. **28**(40), 8983–8989 (2016).
24. A. Kovalsky, L. Wang, G. T. Marek, C. Burda, and J. S. Dyck, "Thermal Conductivity of CH3NH3PbI3 and CsPbI3: Measuring the Effect of the Methylammonium Ion on Phonon Scattering," J. Phys. Chem. C **121**, 3228–3233 (2017).
25. C. C. Stoumpos, C. D. Malliakas, J. A. Peters, Z. Liu, M. Sebastian, J. Im, T. C. Chasapis, A. C. Wibowo, D. Y. Chung, A. J. Freeman, B. W. Wessels, and M. G. Kanatzidis, "Crystal Growth of the Perovskite Semiconductor CsPbBr3: A New Material for High-Energy Radiation Detection," Cryst. Growth Des. **13**, 2722–2727 (2013).
26. X. Li, Y. Wu, S. Zhang, B. Cai, Y. Gu, J. Song, and H. Zeng, "$CsPbX_3$ Quantum Dots for Lighting and Displays: Room-Temperature Synthesis, Photoluminescence Superiorities, Underlying Origins and White Light-Emitting Diodes," Adv. Funct. Mater. **26**, 2435–2445 (2016).
27. M. Kulbak, D. Cahen, and G. Hodes, "How Important Is the Organic Part of Lead Halide Perovskite Photovoltaic Cells? Efficient CsPbBr3 Cells," J. Phys. Chem. Lett. **6**(13), 2452–2456 (2015).
28. E. B. Namdas, M. Tong, P. Ledochowitsch, S. R. Mednick, J. D. Yuen, D. Moses, and A. J. Heeger, "Low Thresholds in Polymer Lasers on Conductive Substrates by Distributed Feedback Nanoimprinting: Progress Toward Electrically Pumped Plastic Lasers," Adv. Mater. **21**, 799–802 (2009).
29. N. Yantara, S. Bhaumik, F. Yan, D. Sabba, H. A. Dewi, N. Mathews, P. P. Boix, H. V. Demir, and S. Mhaisalkar, "Inorganic Halide Perovskites for Efficient Light-Emitting Diodes," J. Phys. Chem. Lett. **6**(21), 4360–4364 (2015).
30. K. Suzuki, A. Kobayashi, S. Kaneko, K. Takehira, T. Yoshihara, H. Ishida, Y. Shiina, S. Oishi, and S. Tobita, "Reevaluation of absolute luminescence quantum yields of standard solutions using a spectrometer with an integrating sphere and a back-thinned CCD detector," Phys. Chem. Chem. Phys. **11**(42), 9850–9860 (2009).

Optics EXPRESS

31. J. Valenta, I. Pelant, and J. Linnros, "Waveguiding effects in the measurement of optical gain in a layer of Si nanocrystals," Appl. Phys. Lett. **81**, 1396–1398 (2002).
32. I. D. W. Samuel and G. A. Turnbull, "Organic Semiconductor Lasers," Chem. Rev. **107**(4), 1272–1295 (2007).
33. G. Murtaza and I. Ahmad, "First principle study of the structural and optoelectronic properties of cubic perovskites CsPbM3 (M=Cl, Br, I)," Phys. B Condens. Matter **406**, 3222–3229 (2011).
34. G. F. Barlow, A. Shore, G. A. Turnbull, and I. D. W. Samuel, "Design and analysis of a low-threshold polymer circular-grating distributed-feedback laser," JOSA B **21**, 2142–2150 (2004).

1. Introduction

Recently, halide perovskite materials, ABX_3 (A = methylammonium (MA), formamidinium (FA), Cs; B = Pb, Sn; X = Cl, Br, I), have rapidly emerged as a series of materials with outstanding optoelectronic performance. These direct band gap materials exhibit large oscillator strengths, long carrier diffusion lengths and low defect densities. Solar cells based on these materials can reach a power conversion efficiency of over 20% [1–3]. On the other hand, owing to their band gap tunability, perovskites also demonstrate great potential in light-emitting applications. Wang *et al.* demonstrated a solution-processed perovskite LED based on self-organized multiple quantum wells exhibiting an external quantum efficiency up to 11.7% [4]. The light-emitting perovskite thin films can be deposited by spin-coating with a subsequent thermal annealing process. By varying the halide anions, the band gap of perovskite can be easily tuned from 1.1 to 3.1 eV, covering the entire visible spectrum and part of the near infrared. Other than thin films, researchers have also demonstrated light-emitting perovskite nanomaterials. Protesescu *et al.* synthesized all-inorganic perovskite nanocrystals with photoluminescence quantum yields (PLQY) up to 90% by hot-injection methods [5]. Hintermayr *et al.* exfoliated perovskite nanoplatelets from bulk materials by ligand-assisted sonication [6].

The radiative efficiency of perovskite thin films is strongly affected by the injected charge-carrier density [7]. Under relatively low carrier density (10^{15} cm^{-3}), the slow bimolecular recombination (10^{-10} cm^3s^{-1} scale) in perovskite films is a fundamental limit for developing high-efficiency LEDs. However, with higher carrier density (> 10^{17} cm^{-3}), the bimolecular recombination and subsequent avalanche can effectively compete with the charge carrier trapping, leading to a much higher radiative efficiency. This means perovskite thin films may become a more promising candidate when used as the laser gain medium, especially for developing electrically pumped lasers in the future.

Since the first demonstration of optically pumped room-temperature amplified spontaneous emission (ASE) and lasing in 2014 [8], perovskite lasers using a broad range of cavities have been demonstrated, including Fabry-Pérot (FP) cavities [9], microplatelets [10], spherical resonators [11], nanowires [12], natural photonic crystal corrugations [13], etc. Compared to micro/nano lasers, which are based on whispering gallery modes (WGM), DFB lasers can achieve a wavelength-tunable single-mode output more easily, and at the same time provide low thresholds, high quality factors and facile manufacturing [14–17]. Lasers working at customized wavelengths with single-mode operation are highly desirable for many practical applications like sensing and communications. In 2016, Brenner *et al*. [18], Saliba *et al.* [19] and Whitworth *et al.* [20] independently reported DFB lasers based on hybrid organic-inorganic perovskite thin films, however, the laser emission of these demonstrations were all located at the near-infrared spectral region. Visible perovskite DFB lasers were demonstrated very recently by Cha *et al.* [21] and Harwell *et al.* [22], both of which were also based on hybrid perovskites.

Here we demonstrate a nanoimprinted DFB resonator using a red-emitting all-inorganic perovskite $CsPbBrI_2$ as the gain medium. Compared to hybrid perovskites, all-inorganic perovskites can achieve higher current densities [23], reduce the heating effects [24], and exhibit better stability against thermal degradation and hydrolysis by atmospheric water [23,25–27]. Besides, the architecture of DFB-integrated light-emitting transistors has been reported as a promising route to achieving an electrically-pumped laser with extremely high

Optics EXPRESS

current densities [28]. All of these merits may benefit to the ultimate goal of developing electrically-pumped lasers. Pumped by a picosecond laser, our microstructured perovskite film shows a emission peak centering at 654 nm with a threshold of 33 μJ/cm^2. The nanoimprint lithography we applied enables a facile and inexpensive way to fabricate DFB resonators, which is also compact with up-scaling and mass production.

2. Solution-processed $CsPbBrI_2$ thin films

The $CsPbBrI_2$ precursor solutions [0.3M in dimethyl sulfoxide (DMSO)] were prepared by mixing $CsPbBr_3$ (CsBr: $PbBr_2$ = 1.2: 1) and $CsPbI_3$ (CsI: PbI_2 = 1.2: 1) solutions with a volume ratio of 1: 2. The excessive amount of CsX was proven to enhance PLQY [29]. Polyethylene oxide (PEO) was then added into the precursor solutions to improve the film quality, resulting in an further enhanced PLQY [23]. The thin films were fabricated by spin-coating solutions onto quartz substrates inside an argon-filled glovebox, followed by a thermal annealing at 70°C for 5 minutes. The absorption and photoluminescence (PL) spectra are presented in Fig. 1(a). The PL curve peaks at 649 nm with a broadband absorption covering a large portion of the UV and visible spectrum. Figure 1(b) compares the PL spectra from a $CsPbBrI_2$-PEO film and a neat $CsPbBrI_2$ film excited at 360 nm with the same absorbance. The PL emission from the neat $CsPbBrI_2$ film is very weak due to the weak exciton binding energy, while the PEO additive enhanced the PL emission by almost an order of magnitude. According to the atomic force microscope (AFM) images of $CsPbBrI_2$-PEO [Fig. 1(c)] and neat $CsPbBrI_2$ [Fig. 1(d)] films, the PEO-treated film shows a much more uniform morphology and smaller grain sizes. The surface roughness was reduced from 24.8 nm to 6.02 nm. This indicates the enhanced PL intensity is attributed to the improved morphology of the $CsPbBrI_2$-PEO thin films, with smaller microcrystalline domains and improved surface smoothness. With the PEO additive, excitons can be confined in small perovskite nanograins with increased exciton binding energies, a process similar to the effects of ligand-stabilized luminescent nanocrystals. Based on Suzuki's method [30], the PLQY of neat film excited at 360 nm was less than 1%, while the value of PEO-treated film was roughly octupled. The XRD patterns of $CsPbBrI_2$-PEO and neat $CsPbBrI_2$ films are shown in Fig. 1(e). The two

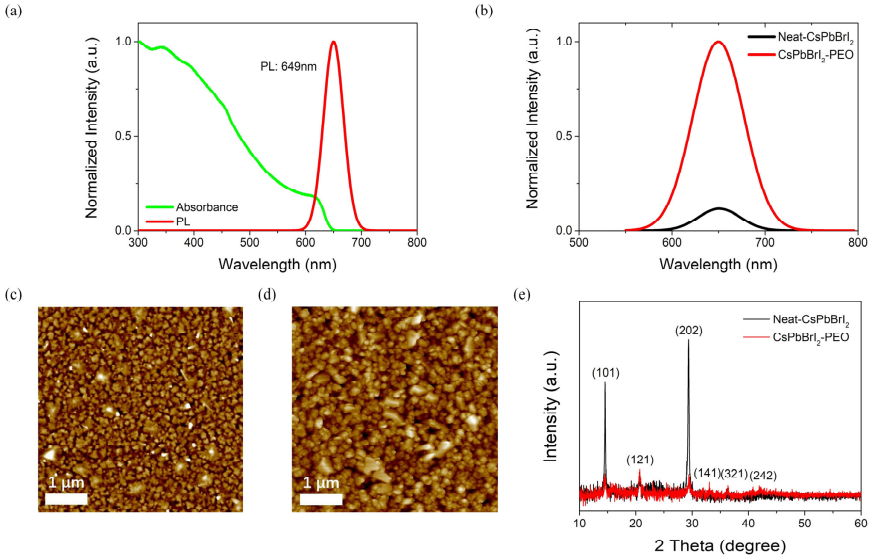

Fig. 1. (a) Absorption and emission spectra of $CsPbBrI_2$-PEO thin films. (b) PL spectra of a $CsPbBrI_2$-PEO film and neat $CsPbBrI_2$ film under the same excitation intensity. AFM images of a (c) $CsPbBrI_2$-PEO film and (d) neat $CsPbBrI_2$ film on quartz substrates. (e) XRD patterns of $CsPbBrI_2$ films with and without the PEO additive.

Optics EXPRESS

patterns are consistent, which indicates the $CsPbBrI_2$ films, with and without the PEO additive, are dominated by the same phase.

The ASE of $CsPbBrI_2$-PEO planar films was observed when the samples were excited at 400 nm with 120 fs pulses at a repetition rate of 1 kHz and with a pump energy of 52 μJ/pulse. As shown in Fig. 2(a), the measured ASE curve centers at 662 nm with a narrowed linewidth of 8.1 nm, while the full-width-at-half-maximum (FWHM) of the spontaneous emission was around 42 nm. Gain and loss coefficients were measured by using the variable-stripe-length (VSL) method [Fig. 2(c)] and shifting-excitation-spot (SES) method [Fig. 2(d)]. The details of the VSL and SES methods can be found in the previous report [31]. The results were shown in Fig. 2(b) and fitted by Eq. (1):

$$I_{VSL}(L,\lambda)-\int_0^L I_{SES}(X,\lambda)dX = A(\lambda)I_P\cdot[\frac{e^{G(\lambda)\cdot L}-1}{G(\lambda)}-\frac{1-e^{-\alpha_{Tot}(\lambda)\cdot L}}{\alpha_{Tot}(\lambda)}], \quad (1)$$

where the $I_{VSL}(L, \lambda)$ is the measured edge-emitting VSL intensity, $I_{SES}(X, \lambda)$ is the SES intensity, X is the excitation spot position with respect to $L = 0$, $A(\lambda)$ is a constant related to the cross section for spontaneous emission, I_p is the pump intensity, $G(\lambda)$ is the net optical gain, and $\alpha_{Tot}(\lambda)$ is the total optical loss due to self-absorption and scattering [32]. The real gain $g(\lambda)$ equals to $[G(\lambda) + \alpha_{Tot}(\lambda)]$. The gain coefficient of the perovskite thin film was found

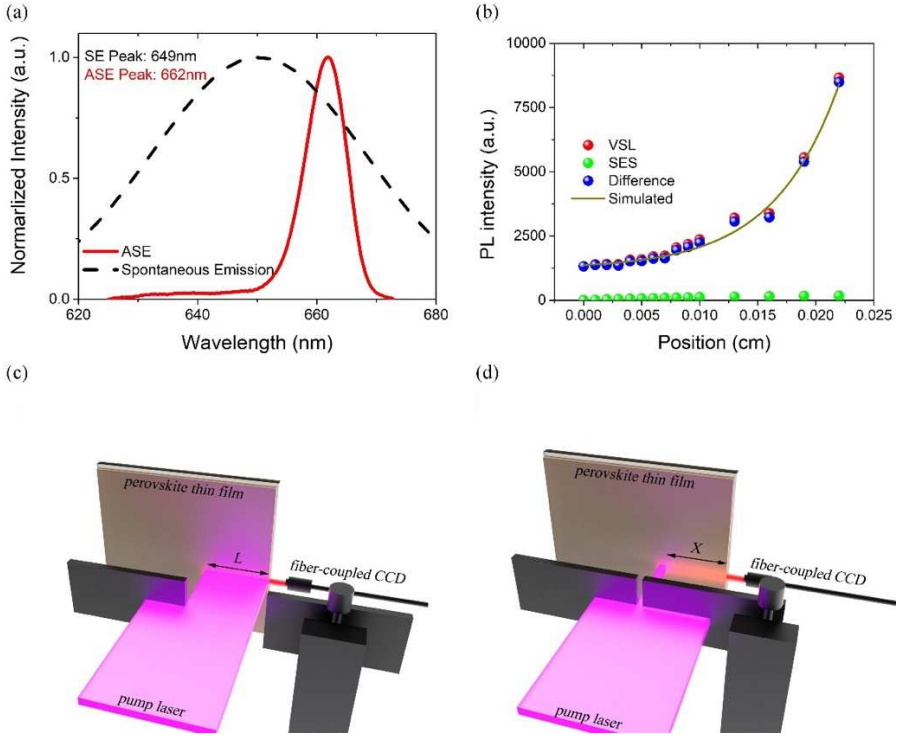

Fig. 2. (a) ASE spectrum of $CsPbBrI_2$-PEO thin films, pumped by a 400 nm laser with 120 fs pulses at a repetition rate of 1 kHz. (b) The measured PL integral intensities against the VSL, and against the distance of the SES. The pump energy was 52 μJ/pulse. Optical gains and losses were acquired by fitting the difference curve of the VSL and SES. A schematic diagram of the (c) VSL method and (d) SES method. For the gain measurement, the pump laser was shaped into a stripe of different lengths and positioned right up to the edge of the sample. For the loss measurement, the length of the stripe was fixed at 2 mm and the stripe was positioned at different distances to the edge. The edge-emission was collected by a fiber-coupled CCD detector.

Optics EXPRESS

to be around 161.1 cm^{-1}, which is close to the value reported in prior work [11]. The loss coefficient was around 30.9 cm^{-1}.

3. DFB laser fabrication and characterization

The schematic diagram of the microstructured all-inorganic perovskite is shown in Fig. 3(a). The system consists of a nanopatterned periodic structure and a perovskite gain layer. The optical feedback is provided by Bragg scattering with an expression of $2n_{eff}\Lambda = m\lambda_{Bragg}$ [16], where n_{eff} is the effective refractive index, Λ is the periodicity, λ_{Bragg} is the Bragg wavelength and m is the order of Bragg scattering. Here we used m = 2 to achieve a surface-emitting signal. Nanopatterned substrates were fabricated by transferring patterns from a binary silicon master grating to hybrid polymer-coated quartz substrates using nanoimprint lithography. As shown in Fig. 3(b), high-quality grating patterns were formed on the substrates, with a period of 360 nm (50% duty cycle), a groove depth of 160 nm and a grating area of 10 mm × 10 mm. Figure 3(c) shows the scanning electron microscope (SEM) image of the $CsPbBrI_2$-PEO coated substrates. The spin-coated film has a thickness of around 80 nm. Eventually, the $CsPbBrI_2$-PEO coated substrates were encapsulated in the glovebox with UV-curable epoxy and glass coverslides.

The sample was then optically pumped by a 355 nm picosecond laser with a repetition rate of 10 Hz and a pulse duration of 90 ps. The excitation beam was focused to a spot of 1 mm radius on the sample. The emission was collected by a monochromator with a single-photon CCD detector. The emission property under different pump energy densities was characterized. Figure 4(a) shows the emission spectra when the sample was pumped below, around and above threshold, indicating a clear linewidth narrowing of emission at the lasing transition. The emission peak above threshold centers at 654 nm with a linewidth of 4.9 nm. For a multilayer slab waveguide consists of an air cladding (n = 1), a 80 nm-thick perovskite core (n = 2.47) [33] and a substrate cladding (n = 1.5), the calculated n_{eff} is 1.816, leading to a

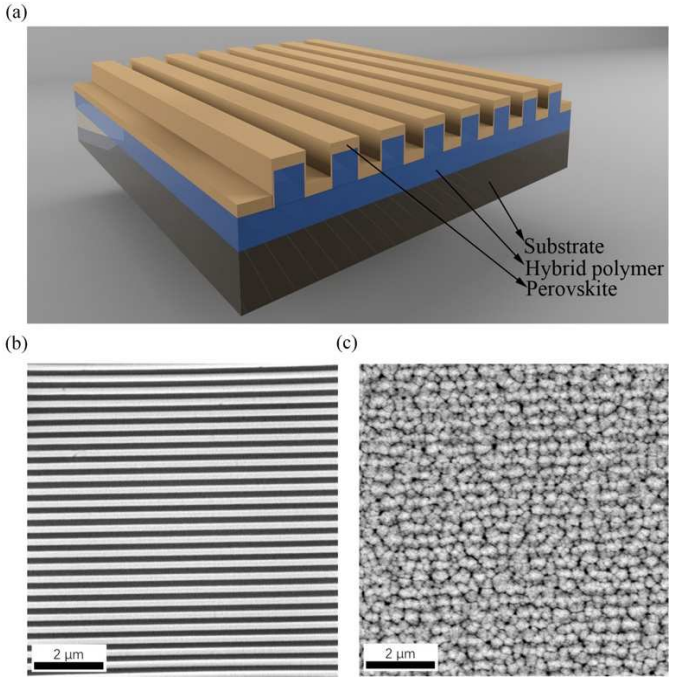

Fig. 3. (a) A schematic diagram of the DFB resonator with an all-inorganic perovskite gain medium. SEM images of the (b) nanopatterned substrates and (c) $CsPbBrI_2$-PEO coated one.

Optics EXPRESS

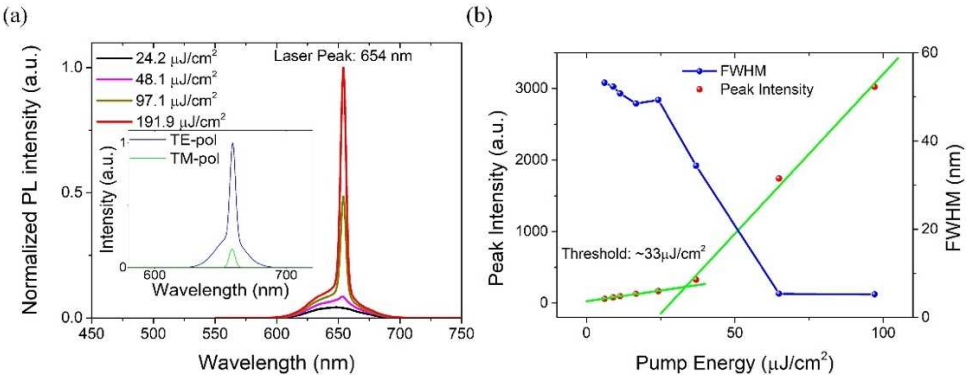

Fig. 4. (a) Emission of the microstructured $CsPbBrI_2$-PEO film at different pump energy densities. The inset shows the polarization of the laser emission. (b) Peak intensity and FWHM as a function of pump energy density.

theoretical lasing peak at 653.7nm, which is almost identical to the experimental results. The emission intensity and linewidth as a function of pump energy density is shown in Fig. 4(b). The change in the slope of the fitted lines determines a threshold of 33 μJ/cm^2, which is in a reasonable range compared to the thresholds of perovskite DFB lasers in prior work [20]. Although all the other characteristics are consistent with lasing, due to the challenges to clearly classify the observed 4.9 nm-linewidth emission is lasing, we decide not to call our observations lasing. We believe the relative wide linewidth is mainly caused by the unfavored duty cycle of the grating. A binary grating with a duty cycle of 50% provides minimal in-plane feedback [34], which is not favorable in our case. A change in duty cycle from 50% to 25% or 75% can form DFB cavities with high-finesse, so the demonstrated microstructured perovskite can potentially achieve a narrower linewidth and lower threshold. In addition, we also fabricated a DFB resonator with neat $CsPbBrI_2$ film as a comparison. We did not observe any lasing behavior, even at very high pump energy densities. This is probably because the non-radiative losses dominate the decay channels in the neat film due to large number of pinholes and high surface roughness.

The polarization of the emission above threshold was distinguished using a polarizer and the results are shown in the inset of Fig. 4(a). The dominant emission in the TE-polarization (the component of the electric field is parallel to the groove direction) indicates the emission

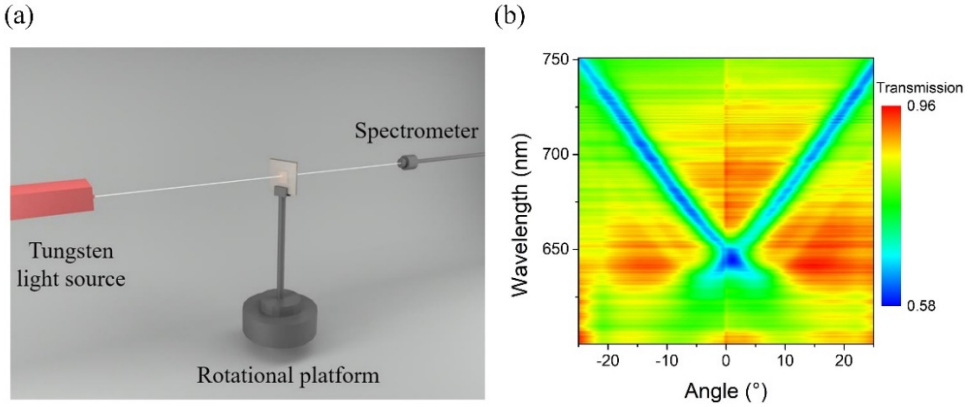

Fig. 5. (a) A schematic diagram of the angle-resolved transmission measurement rig. (b) Angle-resolved transmission spectrum of the microstructured $CsPbBrI_2$-PEO film.

is strongly polarized. The weak signal in the TM-polarization is mainly attributed to the insufficient optical density in the orthogonal polarization of the applied polarizer. According

Optics EXPRESS

to our calculation, a 80 nm-thick $CsPbBrI_2$-PEO can only effectively support the TE_0 waveguide mode, which is consistent with the achieved single-mode emission.

In order to confirm the observed above-threshold emission peak arises from the DFB resonator, an angle-resolved transmission measurement was made using a customized system consisting of a tungsten light source, a rotational platform and a spectrometer. The schematic diagram of the system and the angle-resolved transmission are shown in Fig. 5(a) and 5(b), respectively. The optical resonance wavelength varies with the angle of the incident beam due to the light in-coupling of periodic Bragg structures. The wavelength at the crossing point of the transmission spectrum corresponds to the resonance wavelength at normal incidence (θ = 0°), and the value of around 654 nm matches with the observed lasing peak.

4. Conclusion

In conclusion, we have demonstrated a solution-processed all-inorganic $CsPbBrI_2$ film with a DFB resonator fabricated by nanoimprint lithography. The gain and loss coefficients of the $CsPbBrI_2$ planar film were 161.1 cm^{-1} and 30.9 cm^{-1}, respectively. Excited by picosecond pulses, the microstructured film exhibited a single-mode emission at 654 nm with a threshold of 33 $\mu J/cm^2$. With wavelength-matching Bragg gratings, the halide exchange and mixing of all-inorganic perovskites can potentially realize perovskite lasers covering the entire visible spectrum. This work provides a promising route towards low-cost single-mode visible lasers for applications including displays, high-density data storage and readout, and underwater communications. The unique merits of all-inorganic perovskites may accelerate the development of electrically-pumped lasers.

Funding

National Natural Science Foundation of China (61705042, 51677031, 61378080); Shanghai Sailing Program (16YF1400700); and Engineering and Physical Sciences Research Council (EP/J01771X/1).